# Forward Physics with BRAHMS in pp annd dAu collisions at RHIC

*Dieter Röhrich for the BRAHMS collaboration*
[1]Department of Physics and Technology, University of Bergen, Norway

**Abstract**
Measurements of elementary pp collisions are an integral component to understand heavy ion collisions. Results for pp collisions at 200 and 62.4 GeV are presented. At both energies NLO pQCD describes pion production well. The nuclear modification factor for d+Au collisions at $\sqrt{s_{NN}}$ = 200 GeV changes from a Cronin-like enhancement of pions (and charged hadrons) at midrapidity to an increasing suppression at forward rapidities. In central Au+Au collisions at 200 GeV a strong pion suppression is observed in $R_{AuAu}$ at all rapidities, while protons are enhanced at all rapidities; the nuclear modification factor does not depend on rapidity.

## 1 Nuclear Modification factors

One of the goals of the relativistic heavy ion program is to study the properties of matter at high temperature and high density. The explorations at the Relativistic Heavy Ion Collider (RHIC) indicate that that at c.m. energies of 200 GeV per nucleon pair indeed such system is formed with novel properties [1–4]. Part of these conclusions rely on comparison to elementary pp collisions, where effects of a deconfined matter should not be present.

The high-$p_{\mathrm{T}}$ spectra of particles produced in nuclear collisions are subject to various initial and final state effects. Initial state effects like the Cronin effect enhance the yield in p+A and A+A collisions as compared to nucleon-nucleon reactions at intermediate transverse momenta, nuclear shadowing and gluon saturation suppress the yield. Parton energy loss due to gluon bremsstrahlung during their passage through a dense medium with free color charges - created in central Au+Au collisions - suppresses the hadron yield at high-$p_{\mathrm{T}}$. This final state effect is also called jet-quenching. The degree of suppression/enhancement is quantified by means of the nuclear modification factor $R_{AA}$ using p+p reference spectra scaled up with the average number $N_{coll}$ of binary nucleonic collisions in the heavy-ion system (or by $R_{CP}$ where peripheral collisions are used as a reference):

$$R_{AA} = \left(d^2N_{AA}/dydp_{\mathrm{T}}\right) / \left(N_{coll} \cdot d^2N_{pp}/dydp_{\mathrm{T}}\right). \quad (1)$$

## 2 The BRAHMS experiment

The data used for this analysis were collected with the BRAHMS detector system. The BRAHMS detector consists of two movable magnetic spectrometers, the Forward Spectrometer (FS) that can be rotated from 2.3°to 15°, and the Mid-Rapidity Spectrometer (MRS) that can be rotated from 34°to 90°relative to the beam line, and several global detectors for measuring multiplicities

and luminosity, and determining the interaction vertex, and providing a start time (T0) for time-of-flight measurement. The MRS is a single-dipole-magnet spectrometer with a solid angle of 6 msr and a magnetic bending power up to 1.2 Tm. Most of the pp data presented here were recorded at magnetic field settings of 0.4 and 0.6 Tm. The MRS contains two time projection chambers, TPM1 and TPM2 sitting in field free regions in front of and behind the dipole (D5). This assembly is followed by two highly segmented scintillator time-of-flight walls, one (TOFW) at 4.51 m and a second (TFW2) at either 5.58 m (90°setting) or 6.13 m (other angle settings). The FS consists of 4 dipole magnets D1, D2, D3 and D4 with a bending power of up to 9.2 Tm. The spectrometer has 5 tracking stations T1 through T5, and particle identifying detectors: H2, a segmented time-of-flight wall, and a Ring Imaging Cherenkov Detector (RICH) [5].

## 3 Inclusive pp measurements

The minimum bias trigger used to normalize these measurements is defined with a set of Cherenkov radiators (CC) placed symmetrically with respect to the nominal interaction point and covering pseudo-rapidities that range in absolute value from 3.26 to 5.25. This trigger required that at least one hit is detected in both sides of the array.

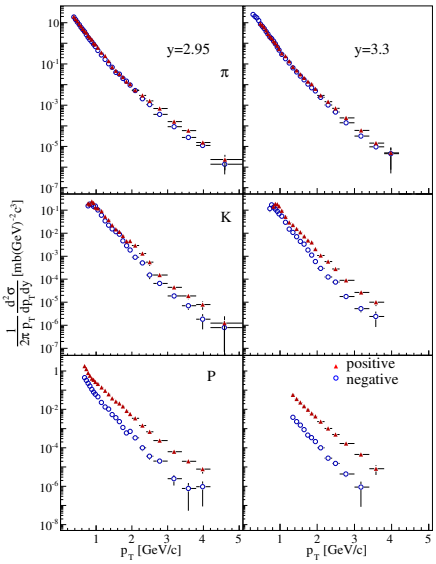


Fig. 1: Invariant cross section distributions for pion, kaons protons and anti-protons produced in p+p collisions at $\sqrt{s} = 200$ GeV at rapidities y=2.95 (left panels) and y = 3.3 (right panels). In all panels, positive charged particles are shown with filled triangles and negative ones with open circles. The errors displayed in these plots are statistical.

The present analysis was done with charged particles that originated from collisions of polarized protons with interaction vertices in the range of $\pm 40$ cm. For the 200 GeV data invariant cross sections were extracted in narrow ($\Delta y = 0.1$) rapidity bins centered at y=2.95 and y = 3.3, respectively. Narrow rapidity bins are required to reduce the effects of rapidly changing cross sections in particular at higher $p_T$. Each distribution is obtained from the merging of up to five magnetic field settings. The data are corrected for the spectrometer geometrical acceptance,

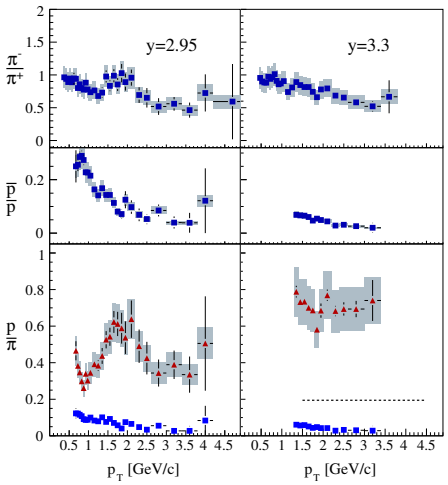


Fig. 2: (Top) Particle ratios versus $p_T$ at y=2.95 and 3.3, (Top) $\pi^-/\pi^+$, (middle) /$K^-$ /$K^+$ and (bottom) proton/$\pi^+$ (red circles) and antiproton/$\pi^-$ (blue squares). The shaded rectangles indicate an overall systematic error (17%) estimated for these ratios. The dashed line shows an upper limit for the (proton + antiproton)/ $\pi^- + \pi^+$ ratio from $e^+e^-$ collisions.

multiple scattering, weak decays and absorption in the material along the path of the detected particles. The overall tracking and track matching efficiency is about 80-90% and is included in the extraction of the cross sections. Particles are identified by the RICH. The low momentum part of the proton spectra is measured using the RICH in veto mode.

Data for y=2.95 and y=3.3 are presented for pions, kaons and protons in Fig.1. The pions exhibit a power law behavior. The upper panels of Fig. 2 show the ratio $\pi^-/\pi^+$ at y=2.95 and 3.3 respectively. Within systematic errors both ratios display a falling trend as a function of $p_T$. This may be an indication of the dominance of valence quark fragmentation at these rapidities and reflects the ratio of d to u quarks in the proton. The antiproton to proton ratios shown in the middle panels are much smaller than unity. This is a clear indication that the fragmententation of gluons cannot dominate the production of protons and anti-protons at these high rapidities. The difference between proton/$\pi^+$ (red circles) and antiproton/$\pi^-$ at both rapidities is remarkable and caused by an unexpectedly large proton yield at these rapidities. Such large yield may be related to the mechanism that transfers a conserved quantity, the baryon number, from beam to intermediate rapidities i.e. baryon number transport. What remains as an open question is how a mechanism that is thought to be mainly restricted to the longitudinal component of the momentum, gives these protons such high transverse momenta.

The measured differential cross-sections are compared with NLO pQCD calculations [6] evaluated at equal factorization and renormalization scales, $\mu \equiv \mu_F = \mu_R = p_T$. These calculations use the CTEQ6 parton distribution functions [7] and a modified version of the "Kniehl-Kramer-Potter" (KKP) set of fragmentation functions (FFs) [8] referred to here as mKKP, as well as the "Kretzer" (K) set [9]. The KKP set includes functions that fragment into the sums $\pi^+ + \pi^-$, $K^+ + K^-$ and proton + antiproton. Modifications were necessary to obtain functions producing the separate charges for both $\pi$ and $K$. Figure 3 shows that the agreement between the NLO calculations that include the mKKP FFs and the measured pion cross section is remarkable (within

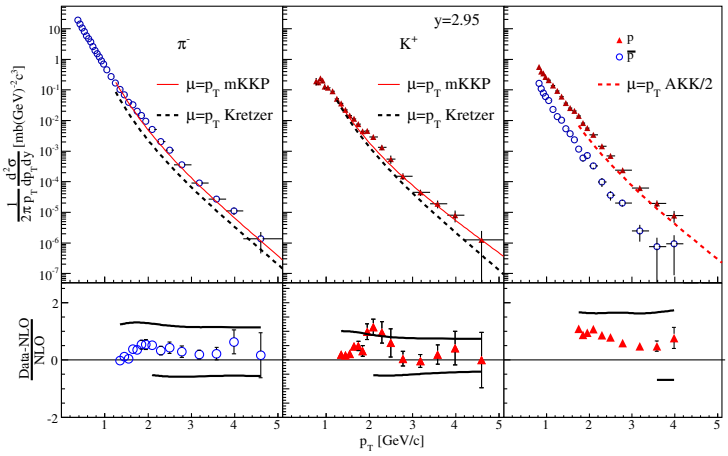


Fig. 3: (Top) Comparison of $\pi^-$ and $K^+$ invariant spectra at rapidity 2.95 to NLO pQCD calculations at 200 GeV. The mKKP set of fragmentation functions (solid red line on-line) produce the best agreement with the pion and kaon data. The protons and antiprotons are compared with the calculation using the AKK set divided by 2 (dashed red line), see text for details. (Bottom) Relative differences between data and calculations. The top smooth curves show the effect of setting $\mu = 2p_T$ and the bottom curves $\mu = 1/2p_T$. For the baryons the (red) filled triangles show proton data vs the AKK/2 set.

20% above 1.5 GeV/c). Similar good agreement was obtained for neutral pions at y=0 [11] and at y=3.8 [12] at RHIC. The agreement between the calculated and the measured kaon cross-sections is equally good. The difference between the mKKP and Kretzer parametrizations is driven by higher contributions from gluons fragmenting into pions. This difference has been identified as an indication that the gg and gq processes dominate the interactions at mid-rapidity [11]. The present results indicate that such continues to be the case at high rapidity. The calculation that uses the Kretzer set underestimates the pion yields by a factor of $\sim 2$ at all values of $p_T$ while for positive kaons the agreement is good at low momentum but deteriorates at higher momenta. An updated version of FFs that we refer to as the "Albino, Kniehl and Kramer" (AKK) set has been extracted from more data made available recently [10]. It reproduces well the proton + antiproton distributions measured at midrapidity by the STAR collaboration [12]. At high rapidity, the contribution from gluons fragmenting into proton or antiproton is dominant in this new set of FFs ( 80% for $p_T$ less than 5 GeV/c [6]), and the calculated cross sections for both particles consequently have nearly the same magnitude. We thus compare the measured cross sections for proton and antiproton to the NLO calculation using the AKK FFs divided by 2 in the right-most panel of Fig. 3. The calculation is close to the measured proton cross section but it is almost an order of magnitude higher than the measured antiproton distribution. We conclude that the AKK FFs cannot be used to describe baryon yields at high rapidity because they fail to reproduce the measured abundance of antiprotons with respect to protons. Additional details can be found in Ref. [13].

At 62.4 GeV, where the beam rapidity is 4.2, the spectrometer at forward angle samples produced particle that carries a significant fraction of the available momenta (31.2 GeV/c). Thus particle production is influenced by the kinematic limit. Data for identified charged hadrons were

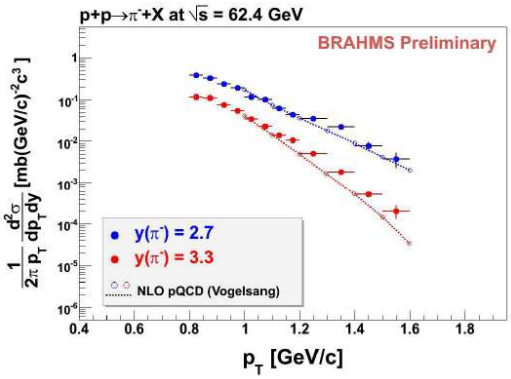


Fig. 4: Invariant cross section for $\pi^-$ at rapidity 2.7 and 3.3 at 62.4 GeV. The curves are NLO pQCD calculations as described in the text.

collected at 2.3°,3°, 4°, and 6°. Figure 4 shows differential cross sections for $\pi^-$ for rapidities 2.7 and 3.3 [14]. The cross sections changes rapidily with rapidity at high $p_T$ where $\mathrm{x}_F$ values up to 0.5 are probed. The data are compared to NLO pQCD in the same figure. The calculation are done in the same manner as for the 200 GeV using the KPP fragmentation function evalauted at $\mu = p_T$ scale. The calculation describe the overall magnitude and shape quite well, though at the highest rapidity there is a tendency for the calculation to fall below the data at the highest $p_T$. This may be in agreement with the analysis [15] of 53 GeV $\pi^0$ data from the ISR at a fixed angle of 5° , comparable to the conditions for present measurements (2.3°and 4°), but at larger $\mathrm{x}_F$ where NLO pQCD is considerably below the data and with increasing discrepancy with $\mathrm{x}_F$. In contrast to the aforementioned paper we do though conclude that NLO pQCD gives a satisfactory description of the charged pion data at high rapidity.

## 4 Nuclear modification factors for cold nuclear matter

Particle production at forward rapidities probes partons at smaller $x$ scales. Suppression effects due to nuclear shadowing and/or gluon saturation are expected in d+Au collisions at large y. Fig. 5 shows the nuclear modification factor $R_{dAu}$ for minimum bias d+Au events as a function of $p_T$ and $\eta$ [16]. $R_{dAu}$ rises with $p_T$ and falls with $\eta$. At midrapidity, $R_{dAu}$ goes above 1. The so-called Cronin enhancement at $\eta = 0$ has been attributed to multiple scattering of the incoming partons during the collision. At more forward rapidities the data show a suppression of the hadron yields.

The suppression at forward rapidities is already visible at SPS energies, $R_{pPb}$ exhibits a similar suppression trend, the suppression increases with increasing $x_F$ [17, 18].

### 4.1 CGC saturation models

Saturation effects should increase with the thickness of nuclear material traversed by the incoming probe and indeed we see a greater suppression for more central collisions [16]. Both, $R_{dAu}$ and $R_{CP}$, as well as the pseudorapidity distribution of charged hadrons and the invariant cross section of $\pi^0$ production in d+Au collisions at RHIC can be quantitatively described by gluon saturation within the framework of a Color Glass Condensate [19, 20].

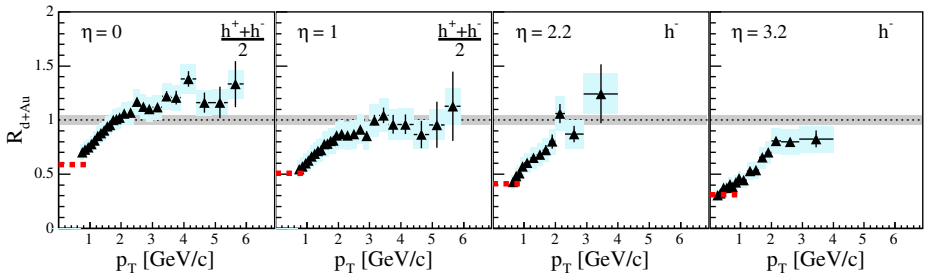


Fig. 5: Nuclear modification factor for charged hadrons at pseudorapidities = 0, 1.0, 2.2, 3.2. One standard deviation statistical errors are indicated by error bars. Systematic errors are shown with shaded boxes. The shaded band around unity indicates the estimated error on the normalization to the number of collisons.

### 4.2 pQCD models

At higher $p_T$ pQCD based models which implement a Glauber-type collision geometry and include the standard nuclear shadowing and initial state incoherent multiple scattering agree reasonably well with the measured $R_{dAu}$ and cannot be ruled out [21] (see also [22]). However, the centrality dependence of $R_{CP}$ is underestimated [23] and there are doubts that nuclear shadowing is strong enough to describe the data [24]. On the other hand, coherent multiple scattering of a parton with the remnants of the nucleus in the final state can create an additional suppression at low and intermediate $p_T$ which grows with rapidity and centrality [25].

### 4.3 Phenomenological models

$R_{dAu}$ has been studied in the framework of Gribov-Regge field theory [26], where shadowing in dAu collisions is linked to diffraction. A parametrized gluonic parton distribution function (data from H1 and ZEUS) can describe the suppression at forward rapidities at RHIC. Applying this model to SPS data, gluonic shadowing, although present at SPS, cannot explain the observed suppression effect at large $x_F$. At SPS energies, shadowing due to valence quarks will dominate in this kinematical region. In general, the large $x_F$ region is dominated by the fragmentation of valence quarks, which may suffer from an induced energy loss via increased gluon bremsstrahlung in cold nuclear matter [27]. In addition, momentum conservation at $x_F \rightarrow 1$ and final state multiple scattering might modify $R_{dAu}$ and $R_{CP}$ (Fig. 6) [27, 28].

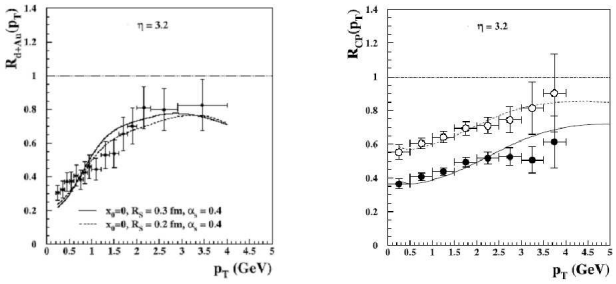


Fig. 6: Suppression due to large $x_F$ effects [27]: $R_{dAu}$ and $R_{CP}$ together with BRAHMS data.

## 5 Final state effects in central nucleus-nucleus collisions

Pion (and charged hadron) transverse momentum spectra at midrapidity in central Au+Au collisions at 200 GeV show a strong suppression at intermediate and high $p_T$ as compared to properly scaled p+p interactions. This effect is attributed to the energy loss partons suffer while traversing the hot and dense medium produced in these collisions.

Fig. 7 compares the (preliminary) nuclear modification factor for pions (left) and protons (right) at midrapidity to the one at forward rapidities [29, 30] (central Au+Au collisions). The pions are clearly suppressed, protons are enhanced and there is no dependence on rapidity.

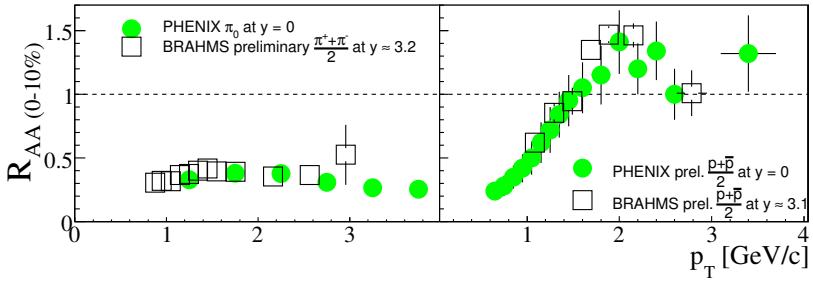


Fig. 7: Preliminary $R_{AuAu}$ for pions (left) and protons (right) at y=0 and y=3 (central Au+Au collisions).

The lack of the rapidity dependence is somewhat surprising since the bulk properties of matter change considerably when going to forward rapidity: the rapidity density of pions drops by a factor of three [31], the radial flow velocity decreases by 30% and the hadron chemistry becomes "SPS-like" [32]. However, a 3D-hydrodynamical simulation starting from a CGC initial condition and including jets [33] can describe both the bulk properties as well as $R_{AuAu}$. The drop of the CGC initial parton distribution by a factor of two and the different time evolution of the thermalized parton density - resulting in less jet energy loss at $\eta = 3.2$ -, is compensated by a steeper $p_T$-slope of the pQCD components at forward rapidities.

An alternative explanation for the constant $R_{AuAu}$ could be that the medium at RHIC is so dense that only particles produced close to the surface can escape and that therefore the corona effect masks the lower parton density at $\eta = 3.2$ [34].

## 6 Conclusion

Unbiased invariant cross sections of identified charged particles as function of $p_T$ were measured at high rapidity in p+p collisions at $\sqrt{s} = 200$ GeV and $\sqrt{s} = 62.4$ GeV. NLO pQCD calculations reproduce reasonably well the produced particle (pions and kaons) distributions.

Suppression phenomena at forward rapidities in d+Au collisions have been seen at RHIC (and SPS); a variety of processes can result in suppression. A strong pion suppression is observed at all rapidities in central Au+Au collisions at 200 GeV, while protons are enhanced at all rapidities ($R_{AuAu}$); the nuclear modification factor does not depend on rapidity.

## References

[1] I. Arsene *et al.*, (BRAHMS collaboration), Nucl. Phys. **A757** 1 (2005).

[2] B. Back *et al.*, (PHOBOS collaboration), Nucl. Phys. **A757** 28 (2005).

[3] J. Adams *et al.*, (STAR collaboration), Nucl. Phys. **A757** 102 (2005).

[4] J. Acox *et al.*, (PHENIX collaboration), Nucl. Phys. **A757** 184 (2005).

[5] M. Adamczyk *et al.*, (BRAHMS collaboration), Nucl. Instrum. Meth. **A499** 437 (2003).

[6] W. Vogelsang, private communication.

[7] J. Pumplin *et al.*, JHEP 0207, 012 (2002); arXiv:hep-ph/0201195.

[8] B.A. Kniehl *et al.*, Nucl. Phys. **B597** 337 (2001).

[9] S. Kretzer *et al*, Eur. Phys. J. **C22** 269 (2001).

[10] S. Albino *et al*, Nucl. Phys. **B725** 181 (2005).

[11] S.S. Adler *et al.*, Phys. Rev. Lett. **91** 241803 (2003).

[12] J. Adams *et al.*, Phys. Rev. Lett. **92** 171801 (2004).

[13] I. Arsene *et al.*, BRAHMS Collaboration. accepted for publication in PRL, arXiv:hep-ex/0701041

[14] F.Videbæk (BRAHMS Collaboration), Proceedings of the 23rd Winter Workshop on Nuclear Dynamics, Bigsky, Montana, 11. - 18. of February, 2007.

[15] C. Bourrely and J. Soffer, *Eur. Phys. J.* **C36** 371 (2004).

[16] I. Arsene *et al.* (BRAHMS collaboration), Phys. Rev. Lett. **93** 242303 (2004).

[17] B. Boimska (NA49 collaboration), PhD thesis, Warzaw (2004).

[18] D. Röhrich, Nucl. Phys. **A774** 297 (2006).

[19] D. Kharzeev, Y. V. Kovchegov and K. Tuchin, Phys. Lett. **B599** 23-31 (2004); D. Kharzeev, E. Levin and M. Nardi, Nucl. Phys. **A730** 448-459 (2004), erratum-ibid. **A743** 329-331 (2004).

[20] A. Dumitru, A. Hayashigaki and J. Jalilian-Marian, hep-ph/0506308.

[21] G. G. Barnafoldi, G. Papp and P. Levai, J. Phys. **G30** S1125-S1128 (2004).

[22] A. Arccadi and M. Gyulassy, J. Phys. **G30** S969-S974 (2004).

[23] R. Vogt, Phys. Rev. **C70** 064902 (2004).

[24] L. Frankfurt, V. Guzey and M. Strikman, Phys. Rev. **D71** 054001 (2005).

[25] J.W. Qiu and I. Vitev, hep-ph/0405068.

[26] K. Tywoniuk *et al.*, Acta Phys. Hung. **A27** 305 (2006).

[27] B. Kopeliovich et al., hep-ph/0501260.

[28] I. Vitev, 2005 RHIC&AGS Annual User's Meeting; T. Goldman, M. Johnson, J.W. Qiu, I. Vitev, in preparation.

[29] P. Staszel *et al.* (BRAHMS collaboration), Nucl. Phys. **A774** 77 (2006).

[30] S.S. Adler *et al.* (PHENIX Collaboration), Phys. Rev. Lett. **91** 072301 (2003).

[31] I. G. Bearden *et al.* (BRAHMS collaboration), Phys. Rev. Lett. **94** 162301 (2005).

[32] I. Arsene *et al.* (BRAHMS collaboration), Acta Phys. Slov. **56** 21 (2006).

[33] T. Hirano and Y. Nara, Nucl. Phys. **A743** 305 (2004); T. Hirano and Y. Nara, Phys. Rev. **C68** 064902 (2003).

[34] A. Dainese, C. Loizides and G. Paic, Eur. Phys. J. **C38** 461 (2005).